

# Microstructure and the Boson-peak in thermally-treated $\text{In}_x\text{O}$ films

Itai Zbeda<sup>1</sup> and Ilana Bar<sup>1</sup> and Z. Ovadyahu<sup>2</sup>

<sup>1</sup>*Physics Department, Ben-Gurion University of the Negev, Beer-Sheva, 8410501 Israel and*

<sup>2</sup>*Racah Institute of Physics, The Hebrew University, Jerusalem 9190401, Israel*

## Abstract

We report on the correlation between the boson-peak and structural changes associated with thermally-treating amorphous indium-oxide films. In this process, the resistance of a given sample may decrease by a considerable margin while its amorphous structure is preserved. In the present study, we focus on the changes that result from the heat-treatment by employing electron-microscopy, X-ray, and Raman spectroscopy. These techniques were used on films with different stoichiometry and thus different carrier-concentration. The main effect of heat-treatment is material densification, which presumably results from elimination of micro-voids. The densified system presents better wavefunction-overlap and more efficient connectivity for the current flow. X-ray, and electron-beam diffraction experiments indicate that the heat-treated samples show significantly less spatial heterogeneity with only a moderate change of the radial-distribution function metrics. These results are consistent with the changes that occur in the boson-peak characteristics due to annealing as observed in their Raman spectra.

PACS numbers:

## INTRODUCTION

Disorder plays a major role in the properties of solids. The study of disorder is a challenge in terms of being able to control, characterize, and quantify it. A significant effort in this vein was invested in the field of electronic transport. In particular, the need for modifying and quantifying disorder is an essential ingredient in the field of disorder-induced phenomena. Prime examples in this category are the metal-insulator transition and the superconductor-insulator transition. The system resistivity is sometimes used as an empirical measure of disorder in these studies. Electric conductivity of a solid is arguably its most sensitive property and it may be affected by different means, not all of them may be attributed to disorder. A change in carrier-concentration for example, naturally affects conductivity while only a small (and indirect) change in disorder may be incurred in the process.

Restricting the lateral dimensions of the sample has been widely used to increase scattering. This is in particular a viable technique to change disorder in transport studies of thin films. However to introduce strong disorder in a three-dimensional system one may have to resort to alloying or use a two-component mixture; a granular system. An effective method that was employed to introduce disorder in a metallic system was exposure to neutron or  $\alpha$ -particle radiation. This technique was employed in modifying the transport properties of A-15,  $\text{MgB}_2$ , and other materials by introducing point-defects and grain-boundary spacing [1].

A complementary, backward procedure is thermal-annealing. This is an effective way to reduce disorder when the system is disordered to start with, a common situation in vacuum deposited or quench-cooled systems. Thermal-annealing has been successfully used in various

transport experiments as a means of fine-tuning the disorder of amorphous indium-oxide ( $\text{In}_x\text{O}$ ) films. It has been shown that thermally-treating  $\text{In}_x\text{O}$  films may result in resistance change of up to 4-5 orders of magnitude at room-temperature with only a small change of carrier-concentration measured by the Hall effect. It seems therefore that the huge change in resistance is due to enhanced mobility, suggestive of a less disordered system. The range of disorder attainable with this method allows studies of both sides of the metal-insulator, and the superconductor-insulator transitions of this material. It was argued that the main reason for the resistance change is densification [2]. This was supported by demonstrating the similarity of the change in the optical-gap during thermally-annealing  $\text{In}_x\text{O}$  films, and in studies of pressure-induced densification of glasses.

Another property known to be sensitive to disorder in solids is the boson-peak (BP), which has been widely studied in amorphous systems and glasses [3–12]. The BP is a feature that appears at the low energy vibrational-density-of-states of amorphous and disordered systems. This feature may be resolved by heat-capacity, neutron scattering experiments, and by Raman spectroscopy. There are several competing theoretical models that purport to account for the mechanism that underlies the BP. The common ingredient in the great majority of them is spatial disorder [4, 5, 8, 13–16]. This makes the characteristics of the BP a relevant probe for monitoring changes in disorder. This is of particular relevance for amorphous systems where quantifying disorder is a challenge. In addition to the lack of long-range order, most amorphous solids exhibit mass density that is lower than their crystalline counterpart. This is presumably due to their being formed by fast cooling from the liquid or gaseous phase [17]. The latter preparation method, quench-cooling the material from the vapor phase onto

a cold substrate, usually results in a porous structure that has many micro-voids reducing the material bulk specific gravity. Consequently, an appreciable volume change may be affected in these structures upon application of pressure, and by thermal-treatment [2].

In this work we attempt to further elucidate these issues using several versions of amorphous indium-oxide as a model system for a metallic glass. This allows us to track changes in the BP due to quantifiable changes of disorder. Raman spectroscopy taken from as-made and annealed  $\text{In}_x\text{O}$  films of different composition, reveal significant changes in the BP magnitude and shape. It is noted that Raman spectroscopy may not faithfully convey the detailed shape of the BP as compared with, for example, heat capacity measurements [18]. However, it is still a viable tool to identify relative changes in the spectra caused by modification of the system structure. Our Raman spectra results are discussed in conjunction with the microstructure information based on X-ray and electron-diffraction experiments made on these samples. In particular, our study illustrates how various aspects of structural disorder affect electronic properties such as conductivity as compared with their effect on the BP shape and magnitude. The similarities and differences with the behavior of the BP in other glasses were pressure was used to modify the structure are pointed out.

## EXPERIMENTAL

### Samples preparation and characterization

The  $\text{In}_x\text{O}$  films were e-gun evaporated onto room-temperature substrates using 99.999% pure  $\text{In}_2\text{O}_3$  sputtering-target. Deposition was carried out at the ambience of  $3\pm 0.5\times 10^{-5}$  to  $4\pm 0.5\times 10^{-4}$  Torr oxygen-pressure maintained by leaking 99.9% pure  $\text{O}_2$  through a needle valve into the vacuum chamber (base pressure  $\simeq 10^{-6}$  Torr). Different substrates were used for the samples prepared for the different measurements techniques. Undoped silicon wafers were used as substrates for electrical measurements, X-ray diffraction (XRD) and Raman spectroscopy measurements. Carbon-coated copper grids were used for transmission electron microscopy (TEM) imaging and electron-diffraction. During deposition and thermal-treatment the grids were anchored to glass-slides by small indium balls pressed onto the glass. The deposited film on the rest of the slide was used for monitoring the sample resistance. X-ray reflectometry (XRR) measurements were performed on samples deposited on 3.8 mm thick float-glass-slides.

Rates of deposition in the range 0.3-2.5 Å/s were used to produce films with different compositions; The  $\text{In}_x\text{O}$  samples had carrier-concentration  $N$  that increases with the ratio of deposition-rate to the oxygen-partial-pressure. For the rates-pressures used here  $N$  was in the

range  $2\times 10^{19}\text{cm}^{-3}$  to  $5\times 10^{21}\text{cm}^{-3}$  as measured by Hall effect at room-temperature using a Hall-bar control-sample prepared simultaneously for each sample deposition. The evaporation source to substrate distance in the deposition chamber was  $45\pm 1\text{cm}$ . This yielded films with thickness uniformity of  $\pm 2\%$  across a  $2\times 2\text{cm}^2$  area. Lateral sizes of samples used for transport measurements was typically  $1\times 2\text{mm}^2$  (width x length respectively), and  $1\times 1\text{cm}^2$  for the Raman spectroscopy. To afford reasonable resolution for electron-microscopy thickness of the films used for TEM work was typically  $d=200\pm 10$  Å.

Three batches of  $\text{In}_x\text{O}$  with different carrier-concentrations  $N=(4\pm 1)\times 10^{19}\text{cm}^{-3}$ ,  $(1\pm 0.5)\times 10^{20}\text{cm}^{-3}$ , and  $(9\pm 1)\times 10^{20}\text{cm}^{-3}$  were used for Raman spectroscopy. For structural analysis we used films characterized by the Ioffe-Regel parameter  $k_F\ell=(3\pi^2)^{2/3}\frac{\hbar\sigma_{RT}}{e^2N^{1/3}}$  in the range of 0.08 to 0.4. Here  $\sigma_{RT}$  is the room-temperature conductivity. This range covers the critical-value of  $k_F\ell=0.32\pm 0.2$  where the metal-insulator transition and superconductor-insulator transition of  $\text{In}_x\text{O}$  take place [19, 20].

High resolution TEM images and electron diffraction patterns were taken with the Philips Tecna F20 G2 operating at 200kV. X-ray diffraction and reflectometry were taken with Bruker diffractometer AXS D8 Advance equipped with Lynexeye XE-T silicon strip-detector. The diffractometer has step resolution of  $10^{-4}\text{deg}$ .

Raman spectroscopy at Ben-Gurion University of the Negev was performed with a home-built ultra-low frequency Raman microscope confocal system that was assembled and optimized for measurements down to  $10\text{cm}^{-1}$ . The setup employed a single longitudinal mode green-laser operating at 532nm. The laser power used in the measurements was typically 3mW for a spot diameter of  $\approx 2.6\mu\text{m}$ . The scattered signal was collected via high throughput 532 longpass nano-edge filters and a single spectrometer [21]. Complementary Raman spectroscopy studies in the Hebrew University were taken with a Renishaw inVia Reflex Spectrometer using a laser beam with either 514 nm or 785 nm wavelength and edge-filter at  $\approx 70\text{cm}^{-1}$  therefore these measurements were limited to energies  $\gtrsim 80\text{cm}^{-1}$ .

### The thermal-treatment protocol

The protocol we routinely use for monitoring the annealing process involves the following steps: After removal from the deposition chamber, the sample was mounted onto a heat-stage in a small vacuum-cell wired to make contacts with the sample for electrical measurements, and a thermocouple attached to the sample-stage as a thermometer. Resistance measurements were performed by a two-terminal technique using either the computer-controlled HP34410A multimeter or the Keithley K617. Next the heating stage is energized, and the resistance and temperature is continuously measured

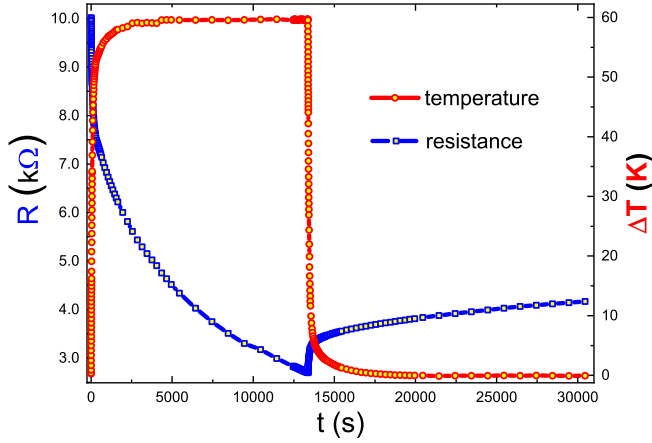


FIG. 1: A typical protocol used in thermal-treating  $\text{In}_x\text{O}$  films. Resistance data  $R(t)$  are shown in squares and refer to the left scale, the sample temperature above room's  $\Delta T(t) \equiv T(\text{heater}) - T(\text{room-temperature})$  is plotted with circles and refer to the right scale. The sample here has  $N \approx 8.5 \times 10^{20} \text{cm}^{-3}$ , thickness of 52nm and lateral dimension of  $1 \times 1 \text{mm}^2$ .

throughout the heating, relaxation, and cooling periods. A typical annealing cycle is illustrated in figure 1:

The sharp changes in the sample resistance  $R$  when the heating is turned on and off are mostly due to the temperature dependent coefficient that in this disorder regime is negative. However, during the time that the temperature has settled at the target value for annealing,  $R$  continues to slowly decrease. Then, after cooldown to room-temperature, the resistance slowly increases approaching an asymptotic value that, ordinarily, is smaller than at the start of the heat-treatment cycle.

These slow  $\Delta R(t)$  reflect changes in the system volume (densification and rarefaction respectively). The change in volume in the process of thermally-treating  $\text{In}_x\text{O}$  films was demonstrated in an interference experiment using grazing-angle X-ray technique [22]. It was further correlated with in-situ resistivity and optical-spectroscopy measurements [22]. For  $\text{In}_x\text{O}$ , a system with the Fermi energy in the conduction band, higher density typically yields higher mobility. This may be due to the enhanced overlap of wavefunctions and improved connectivity. It will be shown below that there is more to the improved mobility than just densification.

The time-dependent processes that occur while the temperature is constant were qualitatively accounted for by a heuristic model based on the two-level-systems that make up the potential landscape of the disordered system [23]. A similar approach was used in [24] to offer a platform for accounting for thermal expansion of glasses.

## RESULTS AND DISCUSSION

### Raman spectra

Figure 2 shows the measured Raman spectra of three batches of  $\text{In}_x\text{O}$  films before and after thermal-treatment. The samples differ by their O-In ratio determined during the deposition process. They are identified in the figure by their carrier-concentration  $N$  measured by the Hall effect. These three compositions were chosen to represent the high- $N$ , medium- $N$  and low- $N$  versions of  $\text{In}_x\text{O}$ . The high- $N$  and low- $N$  versions of  $\text{In}_x\text{O}$  in particular exhibit different behavior in transport [20], and as will be shown below, they differ in terms of other material properties. To cater for the spatial intensity-variations of the scattered signal the Raman spectra were normalized to the intensity of the as-made sample evaluated at  $450 \text{cm}^{-1}$  (averaged value over the interval  $440\text{-}450 \text{cm}^{-1}$ ). This will be referred to as a "background" intensity  $I_0$ . The ratio  $I_P/I_0$ , where  $I_P$  is the intensity at the BP maximum, turns out to be a meaningful measure of the BP magnitude;  $I_0$  taken at different points across a given specimen may vary by more than  $\approx 30\%$  while  $I_P/I_0$  appears to be constant to better than 2% [25].

Qualitatively, the Raman spectra for the three batches in Fig.2 exhibit the same BP shape characteristic of other amorphous and glassy systems [3–16]. There are however two quantitative differences depending on the composition of the material. First, the peak position increases with the O-In ratio (Fig.3). The position of the BP scales with the typical phonon energy of the material which is naturally smaller for the In-richer  $\text{In}_x\text{O}$  so this is just a consequence of the batch composition. That the peak-position appears at a frequency  $\omega_p(\text{O}/\text{In})$  and does not shift due to the thermal-treatment is consistent with the finding that the Hall coefficient is unchanged in the process [2].

Secondly, the heat-treatment causes a more conspicuous decrease of the BP magnitude for the higher- $N$  version while having indistinguishable change in the spectra of the low- $N$  version despite the comparable change in the samples resistance during annealing. Also, for a comparable conductivity, the relative magnitude of the BP, is larger the higher is the carrier-concentration.

The amount of disorder required to affect a given change of the conductivity (or  $k_F \ell$ ) in a degenerate Fermi system like  $\text{In}_x\text{O}$  grows with the Fermi-energy (thus with  $N$ ). This correlation was demonstrated in the dependence of the optical gap on  $k_F \ell$  studied in-situ in [2]. Figure 4 shows three curves from this study for samples with carrier-concentration that are close to these of the batches studied in Fig.2. Note that, for a comparable change of  $k_F \ell$  a larger change of the optical-gap occurred for the sample with the higher carrier-concentration, a similar trend to that observed in the

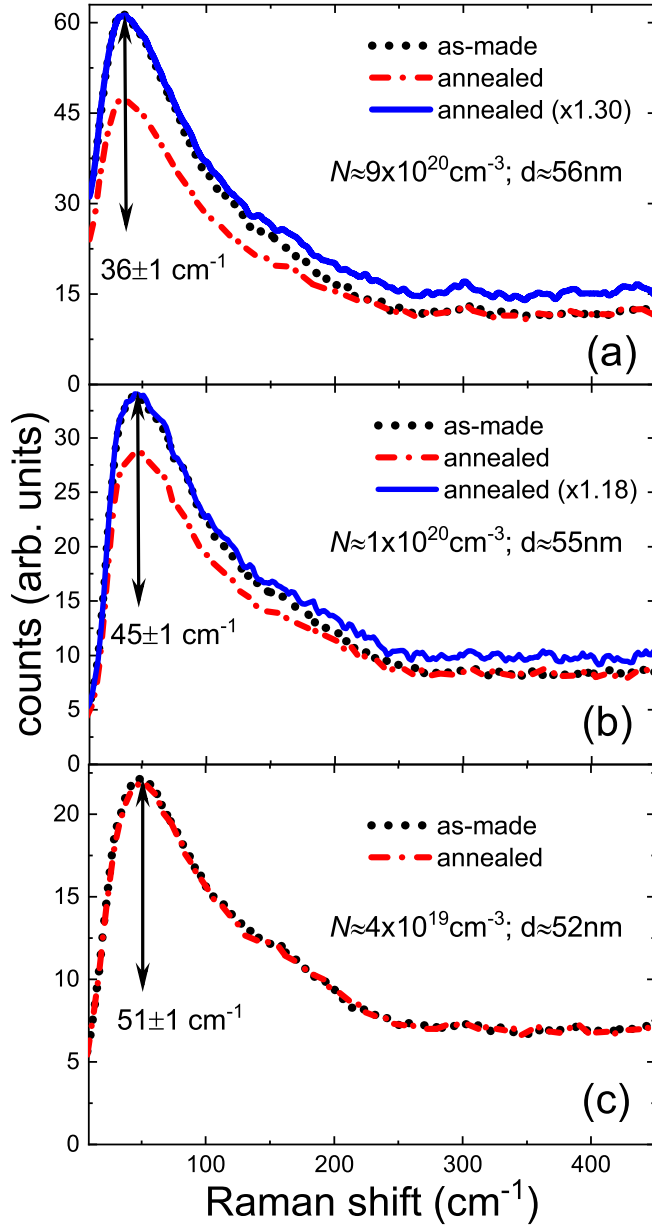


FIG. 2: The Raman spectra for the three studied batches of  $\text{In}_x\text{O}$  measured down to  $\approx 10\text{cm}^{-1}$  with a laser wavelength  $\lambda=532\text{nm}$ . Spectra are shown before and after heat-treatment. The Ioffe-Regel parameters  $k_{\text{F}}\ell$  for these samples are: (a) before-0.11; after-0.39 (b) before-0.12; after-0.41 (c) before-0.078; after-0.42. Blue curves are scaled-up copies of the heat-treated spectra (the factor is chosen to match the intensity reading at the peak). Note that the heat-treated curve shows a wider high-energy tail than the as-made samples of both sample (a) and sample (b).

dependence of the BP on disorder (Fig.2). The relative change of the BP magnitude presumably reflects the degree of the structural-change that occurred during heat-treatment. The correlation between disorder (either chemical or electronic) and  $I_{\text{P}}/I_0$  (table 1) has the same reason - for a comparable  $k_{\text{F}}\ell$  higher disorder yields a

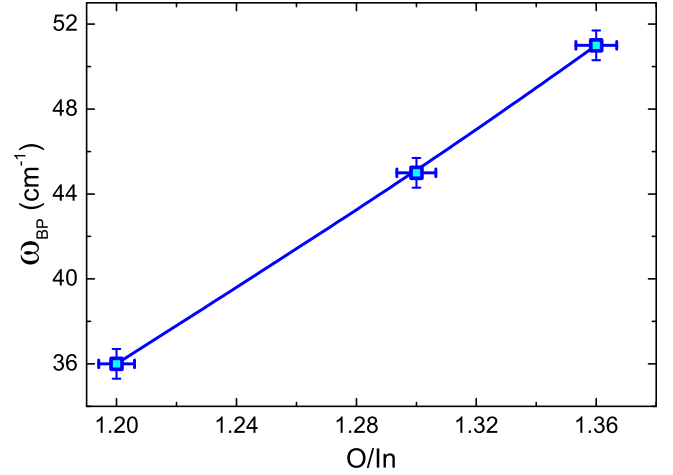


FIG. 3: The dependence of the energy of the BP maximum  $\omega_{\text{BP}}$  on the  $\text{In}_x\text{O}$  composition  $\text{O}/\text{In}$ . This is obtained through the relation between  $N$  and the oxygen/indium mass ratio studied elsewhere (Fig.6 in [19]).

more conspicuous BP demonstrating the common observation related to the phenomenon [12].

Table 1 includes the relative magnitude of the BP before and after annealing, with the batch chemical-disorder  $\delta[\text{O}/\text{In}]$ , and a quantitative measure of disorder  $W_{\text{C}}$  based on data of electronic-transport. The chemical disorder is taken here as the deviation of the composition from that of the stoichiometric  $\text{In}_2\text{O}_3$  compound.  $W_{\text{C}}$  is the critical disorder that Anderson-localizes the particular batch.  $W_{\text{C}} \propto E_{\text{F}} \propto N^{2/3}$  where  $E_{\text{F}}$ , is the Fermi energy. For  $\text{In}_x\text{O}$  the proportionality factor between disorder and Fermi-energy was found to be:  $W_{\text{C}} \simeq 6.2 \cdot E_{\text{F}}$  [2] and  $E_{\text{F}}$  of a given batch is obtained using free-electron formulae.

$\delta[\text{O}/\text{In}]$	$W_{\text{C}}$ (eV)	$I_{\text{P}}/I_0$ as-made	$I_{\text{P}}/I_0$ annealed
0.3	2.21	5.3	4.2
0.2	0.51	4.1	3.4
0.14	0.28	3.1	3.1

Table 1: Values of parameters for the three  $\text{In}_x\text{O}$  batches measured in Fig.2. The electronic disorder (characterized by  $k_{\text{F}}\ell$ ) includes the contribution of the deviation from stoichiometry that may be relevant for phonon scattering vs. electron scattering discussed in the text below. Note the systematic dependence of the BP magnitude on the batch disorder.

### Structural changes resulting from the heat-treatment

Before proceeding with further analysis of the Raman spectra we digress now to see what actually changes in the system micro-structure due to heat-treatment. This

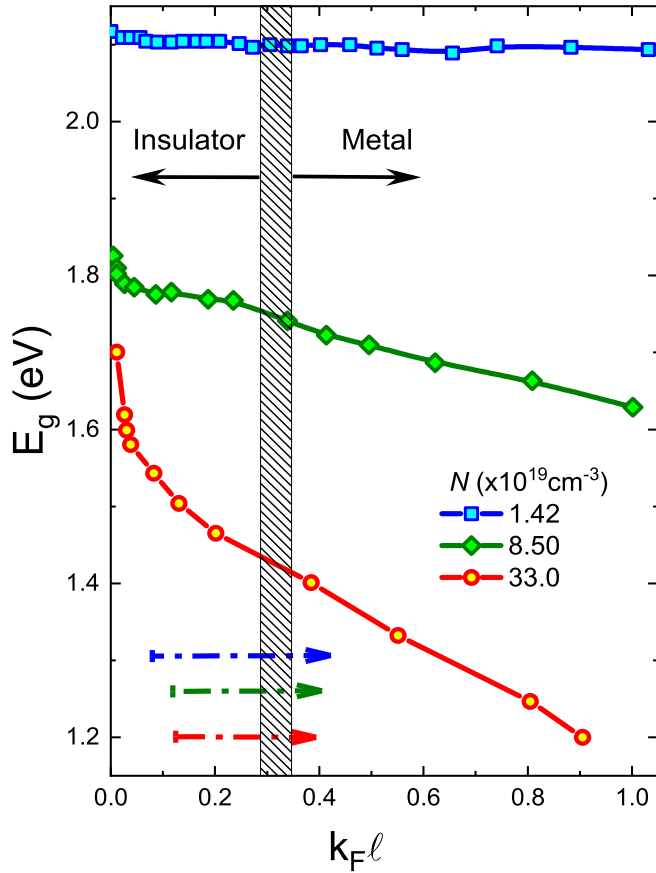


FIG. 4: The dependence of the optical gap on the Ioffe-Regel parameter  $k_F l$  for different versions of  $\text{In}_x\text{O}$  labeled by their carrier-concentration. Note that a larger change of  $E_g$  is required to affect a given change in  $k_F l$  the larger  $N$  is. The arrows mark the value of  $k_F l$  for the as-made and annealed states of the three samples of Fig.2; Red -Fig.2a, Green-Fig.2b, Blue-Fig.2c.

was done by using customary tools of structural analysis; X-ray and electron microscopy. Special emphasis was given to the high- $N$  version of  $\text{In}_x\text{O}$  where the effect in terms of Raman spectroscopy is manifestly large. Consider first the electron-diffraction and TEM images for a typical sample shown in Fig.5a and Fig.5b: Both diffraction patterns exhibit broad rings characteristic of amorphous structure with no sign of crystallization. In fact, it is hard to see difference in the before and after patterns. On closer examination, the first strong ring in the pattern is sharper in the annealed sample and the associated bright-field image appears somewhat softer.

The changes in the diffraction pattern may be quantified by recording the intensity profiles of the diffraction patterns as is illustrated in Figure 6. The measurement confirms the eye-impression; the width of the ring  $\Gamma$  decreased by  $\approx 12\%$  in the annealed sample. At the same time, the average ring-diameter indicated by  $D$  in the figure, *increased* by  $\approx 0.4 \pm 0.1\%$  suggesting a reduced in-

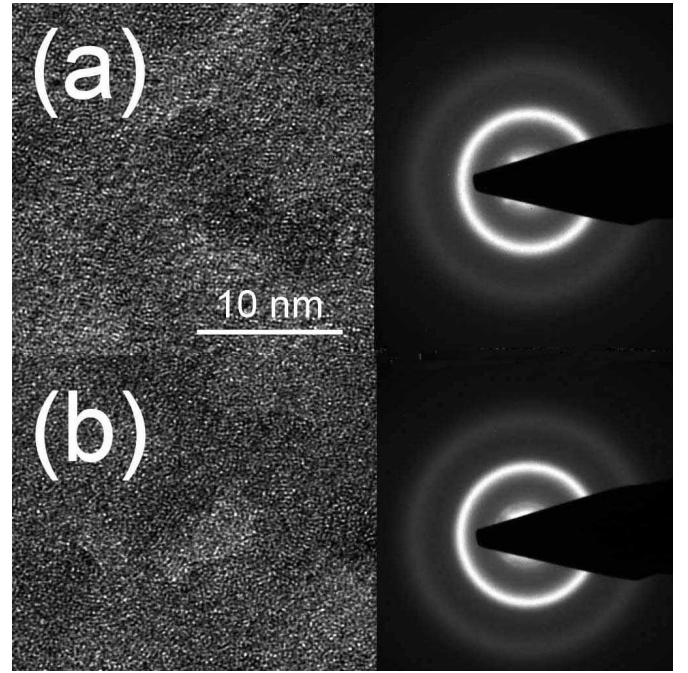


FIG. 5: Bright-field TEM images and the associated diffraction patterns for a 20nm thick  $\text{In}_x\text{O}$  sample deposited on carbon coated Cu grid..(a) as-made and (b) the same sample after heat-treatment. The control sample, deposited on a glass-substrate, had a  $k_F l$  of 0.16 and 0.39 before and after treatment respectively.

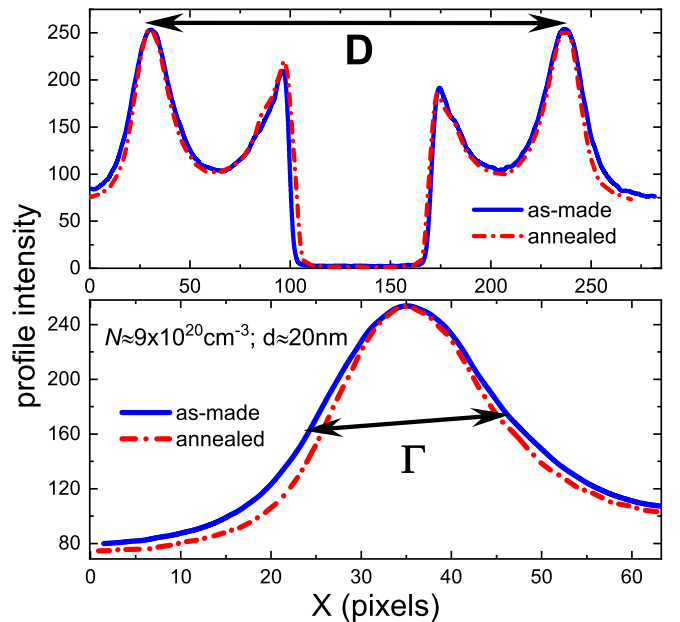


FIG. 6: Intensity profile for the two diffraction patterns shown in Fig.5. Top: Scanned across the first strong ring diameter  $D$ . Bottom: The profile of the first strong ring clearly showing the change in the width  $\Gamma$  after heat-treatment.



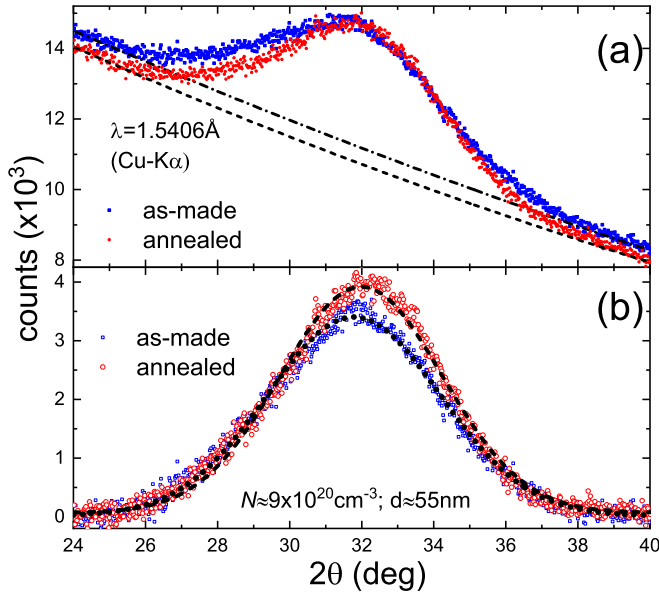


FIG. 7: X-ray diffraction taken over the first strong diffraction ring of the sample that had  $k_F\ell=0.09$  and  $k_F\ell=0.38$  for as-made and annealed samples respectively. (a) Are the raw data, and the dashed and dotted lines stand for the background intensities. These background lines are subtracted from the raw data and fitted in (b) to:  $A \cdot \exp\left[-0.5 \cdot \left(\frac{X-X_0}{\sigma}\right)^2\right]$  where  $A$  is the intensity amplitude and  $X \equiv 2\theta$ . The fits, shown as dashed lines, yield  $X_0=31.78 \pm 0.008$ ;  $\sigma=2.4 \pm 0.01$  and  $X_0=31.98 \pm 0.008$ ;  $\sigma=2.2 \pm 0.01$  for the as-made and annealed plots respectively. The larger intensity at the peak (bottom graph) is due to the reduced background and the narrower line width.

teratomic separation due to annealing.

Similar results were obtained from XRD measurements on this high- $N$  sample as shown in Fig.7. The small differences between the XRD and electron-diffraction in terms of the changes in  $D$  and ring-width may be due to the different substrates used.

On the basis of these measurements one might conclude that the volume-change  $-\Delta V/V$  of this sample due to the thermal-treatment is of the order of 1.2% to 1.8%. However, the results of XRR measurement suggest that  $\Delta V/V$  for this sample may be significantly larger (Fig.8a); Following treatment the sample thickness was reduced by  $\approx 3.3\%$  implying a volume-change  $-\Delta V/V$  of the order of  $\approx 10\%$ . Similar  $-\Delta V/V$  values during heat-treatment were obtained in a previous study of  $\text{In}_x\text{O}$  [2]. The difference in  $-\Delta V/V$  derived from the XRD versus that of the XRR suggest that the  $\text{In}_x\text{O}$  structure is made-up of loosely packed aggregates of relatively dense material. Such a porous medium is common in vapor-deposited films and more generally in substances that were quench-cooled from high temperatures. Actually, porosity is an abundant property of many materials. An extreme example of such a structure is a cotton-ball or

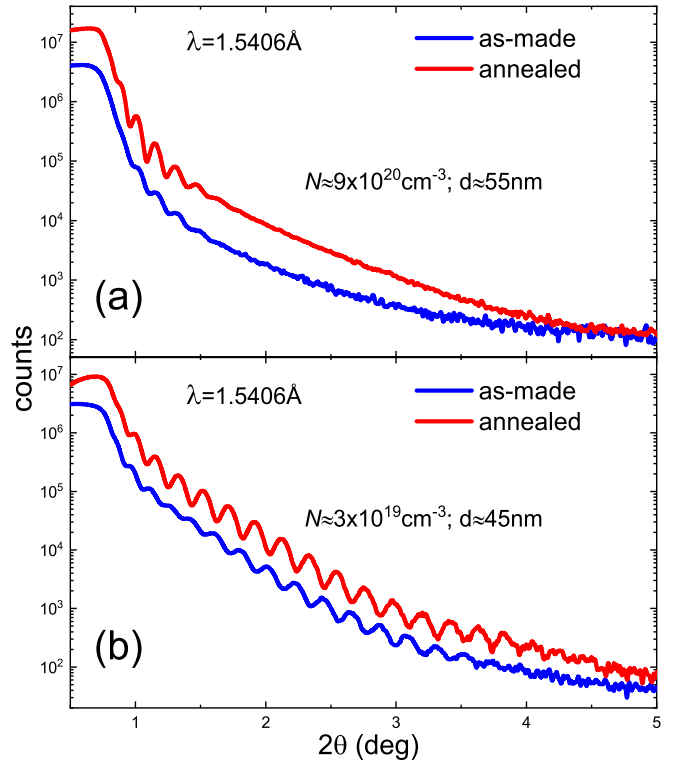


FIG. 8: X-ray reflectometry for two versions of  $\text{In}_x\text{O}$  films having similar composition as that of the samples in Fig.2. Plots are shown for the before-and-after heat-treatment (curves are displaced along the ordinate for clarity). The thickness of the sample in (a) changed during heat-treatment from  $56.2 \pm 0.1\text{nm}$  to  $54.5 \pm 0.1\text{nm}$  and the sample in (b) changed from  $45.1 \pm 0.1\text{nm}$  to  $45 \pm 0.1\text{nm}$ . The films roughness parameters are:  $1 \pm 0.2$  for sample in (a) and  $0.4 \pm 0.1$  for sample in (b).

a bundle of steel-wool. The volume of these substances may be greatly reduced when pressed while their solid part remains essentially intact.

Figure 8b shows the XRR trace taken of a low- $N$  sample that was added for comparison. It exhibits a quantitatively different behavior than the high- $N$  sample in two aspects; the visibility of the interference extends over a wider range of angles, and the change of thickness during heat-treatment is much smaller (per the same change of the sample resistance). Note that heat-treatment enhanced the interference visibility in both samples yet the low- $N$  sample retains a smoother film surface even when its resistance is considerably higher. Evidently, for a similar  $k_F\ell$ , the high- $N$  version of  $\text{In}_x\text{O}$  is both, more disordered and has a rougher surface.

To understand how structural aspects affect conductivity and the BP it may be useful to review the specific ingredients responsible for scattering in  $\text{In}_x\text{O}$  films.

## The elements of disorder in amorphous indium-oxide films and their effect on conductivity and the boson-peak

As amorphous material  $\text{In}_x\text{O}$  lacks long-range order which by itself imposes limit on charge mobility. The vacuum deposited  $\text{In}_x\text{O}$  films have ancillary sources of disorder that lead to scattering and restrict their  $k_F\ell$  value. First, there is an off-diagonal disorder in the material that is related to the distributed nature of the inter-atomic separation. The distribution of inter-particle distances gets narrower as the volume decreases and the system approaches the ‘ideal’ closed-packed amorphous structure. This enhances wavefunction overlap and therefore it naturally affects the conductivity. The diminishment of off-diagonal disorder during heat-treatment is clearly reflected in the reduced width of the electron-diffraction and in the XRD patterns (Figs.5,6 and Fig.7 respectively). The latter has been often associated with the appearance of medium-range order in the system [7]. This re-structure process is also reflected in the rate-distribution of the glass dynamics [23]. The ‘free-volume’ of the sample that is presumably eliminated is probably the most important single element in giving rise to phonon scattering. In fact, a porous nature of amorphous structures has been shown by detailed simulation studies to be the major contributing factor in the BP magnitude [12].

A clear correlation between a structural-change and a modified BP is manifested in our study whenever a significant change of density takes place. This is observed most conspicuously for the heat-treated high- $N$  sample where density is reduced by  $\approx 10\%$  (Fig.8a) and the Raman spectrum shows a  $\approx 30\%$  reduction in magnitude (Fig.2a). The correlation with the material density follows the trend reported in experiments on other disordered systems where the magnitude of the BP was observed to be smaller following densification by pressure [26–35].

The main difference between heat-treatment and applying high pressure appears to be the shift of the BP position to higher energy in the pressure experiments [26–35] whereas no such shift is encountered in the Raman spectra for the thermally-annealed samples. In this regard the evolution of the BP shape in our experiments followed the heterogeneously-distributed elastic-constants scenario described by Schirmacher and Ruocco [8]. A similar behavior to our annealing experiments was observed in the BP spectra of  $\text{As}_2\text{S}_3$  samples after it was cold-quenched from a well-annealed state [36].

Another source of disorder in the amorphous indium-oxide system is associated with deviation from stoichiometry - chemical disorder. Relative to the ionic compound  $\text{In}_2\text{O}_{3-x}$ , there are 5-30% oxygen vacancies in  $\text{In}_x\text{O}$  spanning the range  $\approx 10^{18}$ - $5 \times 10^{21} \text{cm}^{-3}$  in terms of carrier-concentration. To preserve chemical neutrality some in-

dium atoms must assume a valence of +1 instead of the +3 they have in the stoichiometric compound. When randomly distributed this valence-fluctuation forms a background potential with an amplitude of the order of few eV (assuming an average interatomic-separation of the order of  $\approx 0.3 \text{nm}$ ). This type of disorder is quite prevalent in non-stoichiometric compounds, metallic-oxides, high-Tc materials etc. and it seems to be a main source of elastic scattering in both  $\text{In}_x\text{O}$  and  $\text{In}_2\text{O}_{3-x}$  [37]. On the other hand the role chemical-disorder plays in the buildup of a BP is unclear. Deviation from stoichiometry unaccompanied by other factors, does not necessarily promote formation of a BP; Polycrystalline films of  $\text{In}_2\text{O}_{3-x}$  exhibits 5-8% oxygen vacancies [37] while showing very small magnitude of BP relative to the amorphous version [38]. This probably means that oxygen vacancies and larger pockets of free-volume such as di-vacancies, are evenly distributed such that density-fluctuations over a phonon wavelength are rather small.

Finally, the reduction of surface roughness during the heat-treatment revealed in the XRR data needs elaboration. Changes in the interference visibility presumably reflect re-arrangement of ions at the film surface. This seems to occur even when changes in thickness were too small to be observed (see, Fig.8b). In principle, a rough film surface is a source of scattering for both phonons and electrons, and it is natural to expect less scattering when the surface roughness is reduced. Given that the mean-free-path  $\ell$  in our samples is much smaller than the film thickness, the contribution of the surface to scattering by either electrons or phonons is probably very small. Electrical conductivity is sensitive enough to detect a small change of disorder in the sample. For phonons however the same structural change may be too small to affect the BP magnitude (Fig.2c). In other words, a measurable change in conductivity may be affected without a significant structural change, in similar vein with the dependence of the optical-gap  $E_g$  on  $k_F\ell$  for a low- $N$  sample where  $E_g$  remains almost constant while  $k_F\ell$  changes over a large range (Fig.4).

## SUMMARY

We have followed by transport, structural-tools, and Raman spectroscopy the changes that occur during heat-treating  $\text{In}_x\text{O}$  films. Transport measurements were used to quantify the degree of disorder in  $\text{In}_x\text{O}$  samples with different carrier-concentrations before and after treatment. The disorder is characterized by assigning each sample a Ioffe-Regel parameter  $k_F\ell$ . The study reveals a correlation between the system disorder defined in this way, and the magnitude of the BP. This correlation suggests that, in these systems, phonons are scattered by the same elements of disorder that cause scattering of electrons although not necessarily with the same efficiency.

An element of disorder that has a large effect on the BP magnitude is the presence of ‘free-volume’ in the system that, in  $\text{In}_x\text{O}$  is presumably related to the spatial distribution of oxygen vacancies. These are re-arranged during the annealing process to reduce the system volume, and the BP magnitude is changed accordingly. Our study furnishes the experimental support to the simulation work of Shintani and Tanaka that identified the most conspicuous BP in low-density defective structures [12]. This led them to conclude: “...the origin of the boson peak (are) transverse vibrational modes associated with low-density defective structures” [12].

The emerging picture is that heat-treating  $\text{In}_x\text{O}$  is analogous to the process of gently tapping a ground-coffee bag to pack it tighter. Tapping supplies the energy necessary to overcome local barriers allowing the powder to reduce its gravitational energy. Temperature and the interparticle-attraction respectively play the analogous roles in the process of densifying  $\text{In}_x\text{O}$ . Enhanced conductivity due to densification follows from enhanced wavefunction overlap as well as from improved connectivity. This is accompanied by a reduced disorder and therefore weaker heterogeneity which is reflected in a smaller magnitude of the BP. The flexibility that the  $\text{In}_x\text{O}$  system offers in terms of fine-tuning disorder by heat-treatment makes it a prime candidate for the study of electronic transport in glasses, and as demonstrated in this work, also for other fundamental properties of amorphous materials.

We benefitted from discussions with Walter Schirmacher and Alessio Zaccone. The assistance of Anna Radko, Vladimir Uvarov, and Inna Popov from the Center for Nanoscience and Technology (HU) is gratefully acknowledged. This research has been supported by the 1030/16 grant administered by the Israel Academy for Sciences and Humanities.

- 
- [1] H. Wiesmann, M. Gurvitch, A. K. Ghosh, H. Lutz, O. F. Kammerer, and Myron Strongin, Estimate of density-of-states changes with disorder in A-15 superconductors, *Phys. Rev. B* **17**, 122 (1978); M. Gurvitch, A. K. Ghosh, H. Lutz, and M. Strongin, Low-temperature resistivity of ordered and disordered A15 compounds, *Phys. Rev. B* **22**, 128 (1980); M. Putti, R. Vaglio and J. Rowell, Radiation damaged MgB<sub>2</sub>: a comparison with A15 superconductors, *Journal of Physics: Conference Series* **97** 012327 (2008),
- [2] Z. Ovadyahu, Memory versus irreversibility in the thermal densification of amorphous glasses, *Phys. Rev. B* **95**, 214207 (2017).
- [3] V.K. Malinovsky and A.P. Sokolov, The nature of the boson peak in Raman scattering in glasses, *Solid State Com.*, **57**, 757 (1986).
- [4] S. R. Elliott, A Unified Model for the Low-Energy Vibrational Behavior of Amorphous Solids, *EPL* **19** 201 (1992)
- [5] Walter Schirmacher, Gregor Diezemann, and Carl Ganter, Harmonic vibrational excitations in disordered solids and the “boson peak”, *Phys. Rev. Lett.* **81**, 136 (1998).
- [6] N. N. Ovsiuk and V. N. Novikov, Influence of structural disorder on Raman scattering in amorphous porous silicon, *Phys. Rev. B* **57**, 14615 (1998).
- [7] S. Sugai and A. Onodera, Medium-Range Order in Permanently Densified SiO<sub>2</sub> and GeO<sub>2</sub> Glass, *Phys. Rev. Lett.* **77**, 4210 (1996).
- [8] Walter Schirmacher and Giancarlo Ruocco, Heterogeneous Elasticity: The tale of the boson peak, arXiv:2009.05970v1 [cond-mat.dis-nn]
- [9] S. N. Taraskin and S. R. Elliott, Phonons in vitreous silica: Dispersion and localization, *Europhys. Lett.*, **39** (1), 37 (1997).
- [10] J. S. Lannin N. Maley and S. T. Kshirsagar, Raman scattering and short range order in amorphous germanium, *Solid State Com.*, **53**, 939 (1985).
- [11] M. Baggioli and A. Zaccone, Unified theory of vibrational spectra in hard amorphous materials, *Phys. Rev. Research* **2**, 013267 (2020).
- [12] H. Shintani and H. Tanaka, Universal link between the boson peak and transverse phonons in glass, *Nature Mater.* **7**, 870 (2008).
- [13] Vassiliy Lubchenko and Peter G. Wolynes, The origin of the boson peak and thermal conductivity plateau in low-temperature glasses, *PNAS*, **100**, 1515 (2003).
- [14] V. L. Gurevich, D. A. Parshin, and H. R. Schober, Pressure dependence of the boson peak in glasses, *Phys. Rev. B* **71**, 014209 (2005).
- [15] K. Niss, B. Begen, B. Frick, J. Ollivier, A. Beraud, A. Sokolov, V. N. Novikov, and C. Alba-Simionesco, Influence of pressure on the boson peak: stronger than elastic medium transformation, *Phys. Rev. Lett.* **99**, 055502 (2007).
- [16] H. R. Schober, U. Buchenau, and V. L. Gurevich, Pressure dependence of the boson peak in glasses: Correlated and uncorrelated perturbations, *Phys. Rev. B* **89**, 014204 (2014).
- [17] N. F. Mott and A. E. Davis, *electronic Processes in Non-Crystalline Materials*, Oxford University (1971).
- [18] K. A. Blanks, The role of the Raman coupling coefficient in an inelastic light scattering process in amorphous solids, *Journal of Non-Crystalline Solids*, **208**, 81 (1996); A. Fontana, R. Dell’Anna, M. Montagna, F. Rossi, G. Viliani, G. Ruocco, M. Sampoli, U. Buchenau and A. Wischniewski, The Raman coupling function in amorphous silica and the nature of the long-wavelength excitations in disordered systems, *Europhys. Lett.*, **47**, 56 (1999); Bernhard Schmid and Walter Schirmacher, Raman Scattering and the Low-Frequency Vibrational Spectrum of Glasses, *Phys. Rev. Lett.* **100**, 137402 (2008).
- [19] D. Shahar and Z. Ovadyahu, Superconductivity near the Mobility Edge, *Phys. Rev. B* **46**, 10917 (1992).
- [20] U. Givan and Z. Ovadyahu, Compositional disorder and transport peculiarities in the amorphous indium-oxides, *Phys. Rev. B* **86**, 165101 (2012).
- [21] See Supplemental Material at [URL will be inserted by publisher] for fuller details of the two setups used for Raman spectroscopy and associated data.
- [22] Z. Ovadyahu, Slow dynamics of the electron-glasses; the role of disorder, *Phys. Rev. B*, **95**, 134203 (2017).
- [23] Z. Ovadyahu, Structure dynamics in thermal-treatment



of amorphous indium-oxide films, *Phys. Status Solidi B* **257**,1900310 (2020).

- [24] Yu. M. Galperin, V. L. Gurevich and D. A. Parshin, Theory of low-temperature thermal expansion of glasses, *Phys. Rev.B* **32**, 6873 (1985).
- [25] See figure S4 in Supplemental Material at [URL will be inserted by publisher] for an example.
- [26] L. Orsingher, A. Fontana, E. Gilioli, G. Carini, G. Carini, G. Tripodo, T. Unruh, and U. Buchenau, Vibrational dynamics of permanently densified GeO<sub>2</sub> glasses: Densification-induced changes in the boson peak, *J. Chem. Phys.* **132**, 124508 (2010).
- [27] T. Deschamps, C. Martinet, D. de Ligny, J. L. Bruneel, and B. Champagnon, Correlation between boson peak and anomalous elastic behavior in GeO<sub>2</sub> glass: An in situ Raman scattering study under high pressure, *J. Chem. Phys.* **134**, 234503 (2011).
- [28] J. Schroeder, W. Wu, J. L. Apkarian, M. Lee, L.-G. Hwa, C. T. Moynihan, Raman scattering and Boson peaks in glasses: temperature and pressure effects, *J. Non. Cryst. Solids* **349**, 88 (2004).
- [29] M. Ahart, D. Aihaiti, R. J. Hemley, and Seiji Kojima, Pressure dependence of the Boson peak of glassy glycerol, *J. Phys. Chem. B* **121**, 6667 (2017).
- [30] B. Mantisi, S. Adichtchev, S. Sirotkin, L. Rafaely, L. Wondraczek, H. Behrens, C. Marcenat, N. V. Surovtsev, A. Pillonnet, E. Duval, B. Champagnon, and A. Mermet, Non-Debye normalization of the glass vibrational density of states in mildly densified silicate glasses, *J. Phys.: Condens. Matter* **22**, 025402 (2010).
- [31] V. L. Gurevich, D. A. Parshin, and H. R. Schober, Pressure dependence of the boson peak in glasses, *Phys. Rev. B* **71**, 014209 (2005).
- [32] L. Hong, B. Begen, A. Kisliuk, C. Alba-Simionesco, V. N. Novikov, and A. P. Sokolov, Pressure and density dependence of the boson peak in polymers, *Phys. Rev. B*, **78**, 134201 (2008).
- [33] M. Zanatta, G. Baldi, S. Caponi, A. Fontana, E. Gilioli, M. Krish, C. Masciovecchio, G. Monaco, L. Orsingher, F. Rossi, G. Ruocco, and R. Verbeni, Elastic properties of permanently densified silica: A Raman, Brillouin light, and X-ray scattering study, *Phys. Rev. B* **81**, 212201 (2010).
- [34] A. Monaco, A. I. Chumakov, G. Monaco, W. A. Crichton, A. Meyer, L. Comez, D. Fioretto, J. Korecki, and R. Rüffer, Effect of densification on the density of vibrational states of glasses, *Phys. Rev. Lett.* **97**, 135501 (2006).
- [35] E. Stavrou, C. Raptis, and K. Syassen, Effects of pressure on the boson peak of tellurite (TeO<sub>2</sub>)<sub>1-x</sub>(ZnO)<sub>x</sub> glasses: Evidence of an elastic glass-to-glass transition, *Phys. Rev. B* **81**, 174202 (2010).
- [36] V.K. Malinovsky and A.P. Sokolov, The nature of the boson peak in Raman scattering in glasses, *Solid State Com.*, **57**, 757 (1986).
- [37] Z. Ovadyahu, B. Ovrin and H.W. Kraner, Microstructure and electro-optical properties of evaporated indium-oxide Films, *J. Elect. Chem. Soc.* **130**, 917 (1983).
- [38] See figure S3 in [21].

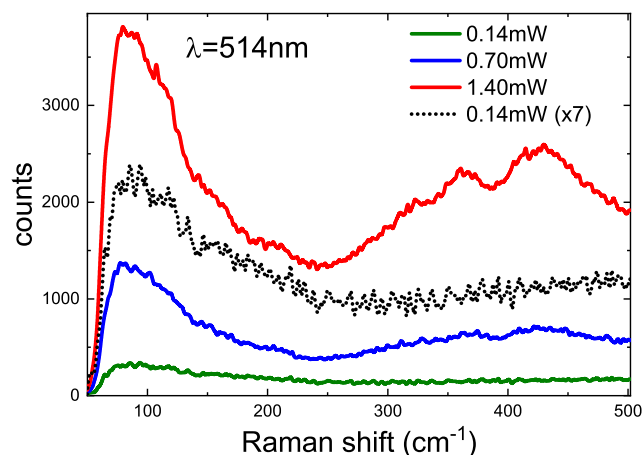


FIG. 9: Raman spectra taken consecutively on a single spot with different laser powers. The sample is a 20nm In<sub>x</sub>O film deposited on a carbon-coated TEM copper grid. Note the appearance of extra structure for the 0.7mW plot that gets further developed for the 0.14mW exposure.

## SUPPLEMENTARY MATERIAL

This part and the following subsections give auxiliary information related to the methods and techniques employed in the study.

### Avoiding crystallization

One should realize that the crystalline version of indium-oxide, In<sub>2</sub>O<sub>3-x</sub> differs markedly from these amorphous versions that are investigated here. In<sub>x</sub>O may be easily crystallized to form polycrystalline In<sub>2</sub>O<sub>3-x</sub> once exposed and maintained at temperatures as low as 380K (depending on the In<sub>x</sub>O composition). The danger of In<sub>x</sub>O crystallization must be taken into account especially when exposing the film to intense laser radiation but also during heat-treatment. Keeping the heat-treatment temperature below 370K practically eliminates crystallization problems; we never encountered a problem with heat-treatment even when the sample was left for 34 days at this temperature. It is more complicated to set a limit for the laser power because it depends on the heat-dissipation through the substrate. To assist in identifying the threshold we carried an experiment designed to observe the onset of structural changes using high-resolution TEM. The results are shown in Fig.9 and Fig.10:

On the basis of the correlation between these structural and Raman data we identify the spectra taken with 0.7mW and 1.4mW laser power as a signature of partial crystallization, or a highly defected polycrystalline phase (see Fig.11 for typical spectrum of well-annealed In<sub>2</sub>O<sub>3-x</sub> that lacks the pronounced BP observe in the

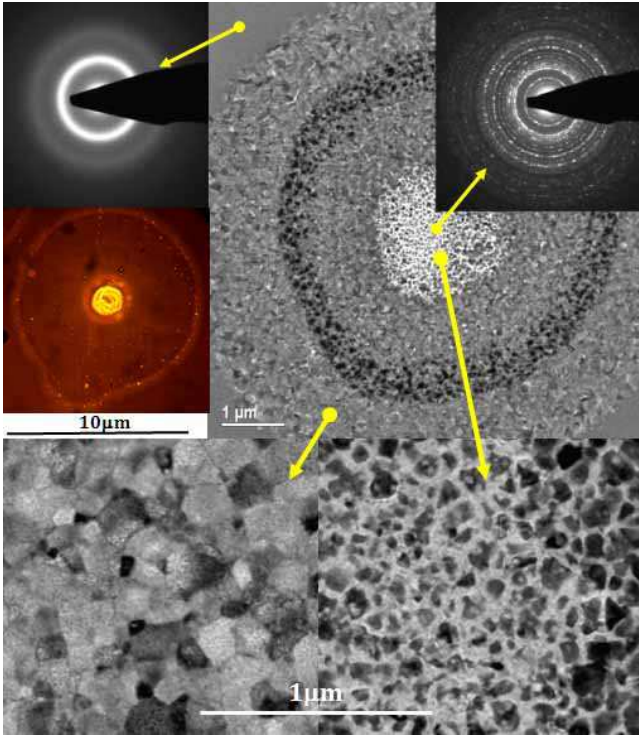


FIG. 10: TEM and optical microscope pictures of the spot created by the laser exposures in SM1 above. The arrows mark the local area from which either bright-field image or diffraction pattern were taken. Note that the structural effect of the  $2\mu\text{m}$  laser-spot extends over  $\approx 10\mu\text{m}$ . The sample is a  $\approx 2\text{nm}$   $\text{In}_x\text{O}$  deposited on carbon-coated copper grid.

laser-exposed plots in Fig.9). This signature was used in the study to set the power-limit on samples deposited on Si-wafers. The latter exhibit more efficient heat-dissipation than the carbon film used for the TEM work allowing a larger laser power to be used (see text).

### Low-energy Raman setup

A home-built ultra-low frequency Raman confocal system was assembled and optimized for measurements of Raman spectra down to  $10\text{cm}^{-1}$ . The setup included an exciting-source Nd:YAG laser (CNI, MSL-FN-532), and the scattered signal was collected via high throughput 532 longpass nano-edge filters (NEFs) and a single spectrometer.

In particular, a single longitudinal mode doubled Nd:YAG laser (CNI, MSL-FN-532) beam from a diode-pumped solid-state laser was directed toward a reflecting Optigrate band-pass filter, based on the volume Bragg-grating technique for cleaning up the laser spectral noise and resulting in spectral widths  $< 7\text{cm}^{-1}$ . Then two mirrors were used to aim the reflected laser beam towards a 532 NEF (Iridian spectral technologies) with deep blocking ( $> \text{OD } 6$ ) at the laser line, set in an adjustable filter

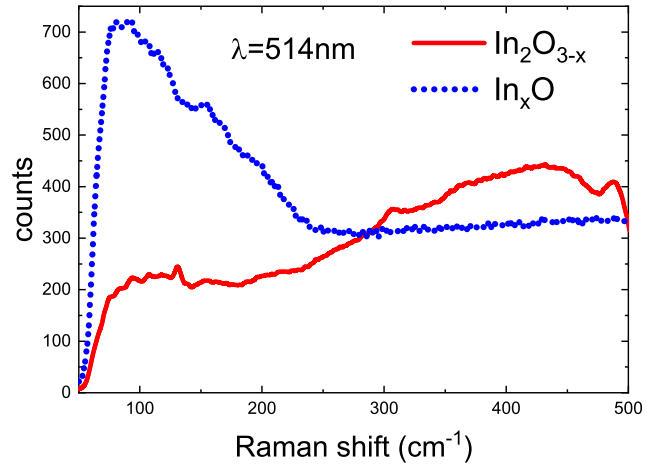


FIG. 11: Raman spectra of two distinct structures of indium-oxide. The plot labeled as  $\text{In}_2\text{O}_{3-x}$  (red-line) is crystallized from the deposited amorphous film with thickness  $90\text{nm}$  to form the polycrystalline version of indium-oxide. The blue dotted line depicts the spectrum taken from the deposited  $\text{In}_x\text{O}$  film. The substrate is quartz.

holder. The combination of the mirrors with the NEF1, allowed to adjust the angle between the incident laser beam and the normal of NEF1 for gaining the best laser line attenuation and the lowest possible frequency of the ULF Raman signal, as well as to reflect the beam to the microscope objective. The laser beam was focused through a X50/0.65 microscope objective to provide a  $3\text{mW}$  incident beam on the sample, which also collected and collimated the back scattered Rayleigh and Raman signals. The backscattered signal passed through the above mentioned NEF1, partially filtering the signal and then through an additional filter, NEF2, to achieve the desirable attenuation of the Rayleigh signal. Following the passage through the filters, the signal was focused by a  $10\text{cm}$  focal length plano-convex lens onto a pin-hole ( $100\mu\text{m}$ ), located in front of a  $10\mu\text{m}$  slit of a  $0.14\text{m}$  Czerny-Turner spectrometer (Jobin-Yvon, MicroHR) with an entrance aperture ratio of  $f/3.88$ , with a  $1200\text{g/mm}$  grating. Finally, the signal was detected by an air cooled  $1,024 \times 1,024$  intensified charge-coupled device (Andor, DH734-18U), driven by the Solis 4.3 software and analyzed. The system can achieve spectral resolution at the full-width half-maximum of a peak in the spectrum of up to  $11\text{cm}^{-1}$ . The spectra of the samples mentioned below were measured under similar conditions with the detector operated at integration times of  $15\text{min}$ .

### Spectra normalization

To get a good signal to noise and avoid risk of crystallization calls for compromises. The laser spot used had a diameter of  $2\mu\text{m}$  (Renishaw setup) and  $2.7\mu\text{m}$  (BGU

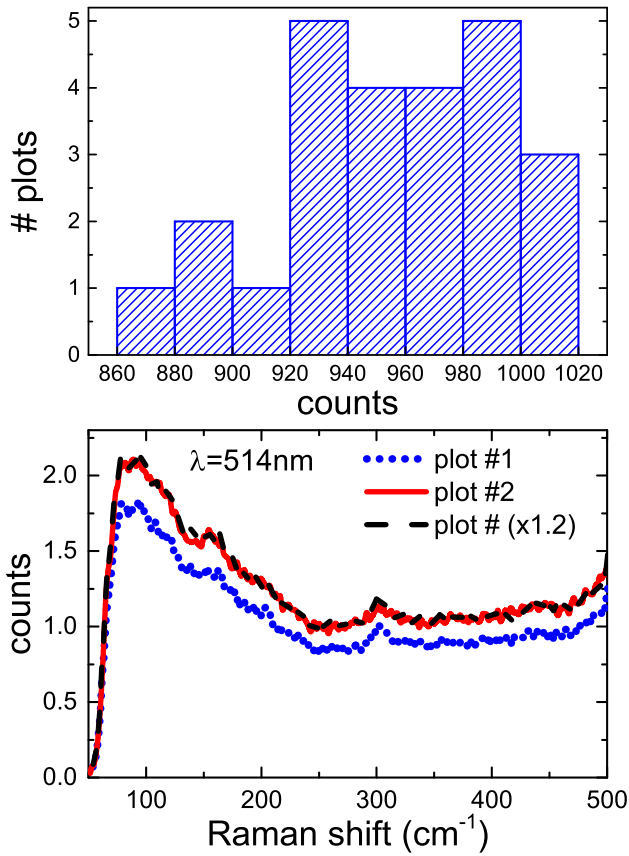


FIG. 12: Top: Histogram of the 25 local-intensities of IR signal taken on a 55nm  $\text{In}_x\text{O}$  film (see text). Bottom: Raman spectra taken from two local readings with extreme low-high intensities in the histogram and illustrating that they only differ by a numerical factor.

setup) and the question of sample uniformity being typically  $1 \times 1 \text{cm}^2$ , had to be tested. Taking advantage of the computerized Invidia (Renishaw) features, several runs of 25 spots on a sample were taken for statistics purposes. These 25 scans were taken consecutively on a  $0.1 \times 0.1 \text{mm}$  square (5 rows, 5 columns). The Raman signal in the interval  $440\text{-}450 \text{cm}^{-1}$  was averaged for each of the 25 traces and the histogram of these values is shown in Fig.12:

The figure also includes the spectra for two traces for which the variation in the magnitude of the signal is the greatest and it is illustrated that they can be made to overlap by multiplying by a constant factor. On basis of such measurements we opted for normalizing the curves using  $I_0$  as the reference (see Fig.2 of the main text).